Attosecond timing the ultrafast charge-transfer process in atomic collisions

S. X. Hu (胡素兴)[*]

Laboratory for Laser Energetics, University of Rochester, 250 East River Road, Rochester, New York 14623, USA
(Received 2 September 2010; published 14 April 2011)

By solving the three-dimensional, time-dependent Schrödinger equation, we have demonstrated that the ultrafast charge-transfer process in ion-atom collisions can be mapped out with attosecond extreme uv (xuv) pulses. During the dynamic-charge transfer from the target atom to the projectile ion, the electron coherently populates the two sites of both nuclei, which can be viewed as a "short-lived" molecular state. A probing attosecond xuv pulse can instantly unleash the delocalized electron from such a "transient molecule," so that the resulting photoelectron may exhibit a "double-slit" interference. On the contrary, either reduced or no photoelectron interference will occur if the attosecond xuv pulse strikes well before or after the collision. Therefore, by monitoring the photoelectron interference visibility, one can precisely time the ultrafast charge-transfer process in atomic collisions with time-delayed attosecond xuv pulses.

The generation of attosecond extreme uv (xuv) pulses [1–3] through high-harmonic generation [4,5] from atoms and molecules driven by intense few-cycle pulses (FCPs) [6] has opened an active research field of attosecond sciences [7–11]. Working much as a strobe light that can help capture stop-action photographs of racehorses, attosecond xuv pulses can freeze the even faster motion of electrons within atoms and molecules. In the past several years, attosecond xuv pulses have been used to measure the ultrafast Auger decay of atoms [12] in real time, the electric-field oscillations within an FCP [13], and the dynamic electron tunneling within molecules [14], and also to explore electron correlations inside atoms and molecules [15–19].

It is well known that electrons released by intense optical pulses can scatter off their "parent" atoms or molecules, thereby leading to the so-called "target self-imaging" with intense FCPs [20–25]. Most recently, it has also been shown that instantly "unleashed" photoelectrons from molecular targets, when struck by intense attosecond xuv pulses, can elucidate the transient molecular structures by resembling a "double-slit" interference [26–28]. This kind of attosecond photoelectron microscopy (APEM) may find a variety of applications for imaging ultrafast processes in nature. In this Rapid Communication, we will demonstrate that the ultrafast charge-transfer process in atomic collisions, occurring at a time scale of hundreds of attoseconds, can be mapped out with APEM. Namely, by striking the ion-atom colliding system with time-delayed attosecond xuv pulses, one can monitor the photoelectron interference visibility to timing the exact moment when the charge transfer occurs. This would enable us not only to explore such ultrafast processes but also to gain further control of collisional reactions in physical and chemical systems.

To investigate the feasibility of attosecond timing the ultrafast charge-transfer process in atomic collisions [29], we numerically solve the three-dimensional (3D), time-dependent Schrödinger equation (TDSE). As an example, the atomic collision of a deuterium ion (D^+) with a target hydrogen atom

(H) is considered here. Under the straight-line approximation [30] for the projectile ion D^+, the TDSE governing the collisional electron dynamics and the attosecond xuv probing can be written as [atomic units (a.u.) used throughout]

$$
i \frac{\partial}{\partial t} \Psi(x,y,z;t) = \left[-\frac{1}{2} \left(\frac{\partial^2}{\partial x^2} + \frac{\partial^2}{\partial y^2} + \frac{\partial^2}{\partial z^2} \right) \right.
$$
$$
- \frac{1}{\sqrt{x^2 + y^2 + z^2}}
$$
$$
- \frac{1}{\sqrt{(x - x_0 - vt)^2 + (y - y_0)^2 + (z - z_0)^2}}
$$
$$
\left. + x E(t) \right] \Psi(x,y,z;t), \tag{1}
$$

where the projectile D^+ having a kinetic energy E_k starts at (x_0, y_0, z_0) with a velocity of v moving toward the positive x axis, while the target H atom on its ground state is located at the origin. The probing attosecond xuv pulses, linearly polarized along the x axis, may strike the colliding system at any given instant. The xuv pulse field $E(t)$ has a Gaussian-like envelope with a pulse duration of 100 attoseconds (as) and a photon energy of $\hbar\omega \approx 200$ eV. The peak field strength is ~ 3.7 a.u. To solve Eq. (1), we have employed the finite-element discrete-variable-representation (FEDVR) scheme combined with the real-space-product (RSP) propagator [31,32]. The RSP-FEDVR code has been applied for studying atomic and molecular dynamics when exposed to intense optical and xuv pulses [22,26,33], as well as for exploring three-body electron-ion recombinations [34] and electron-Rydberg atom collisions [35].

For the fast projectile D^+ with an energy of $E_k = 10$ keV and its initial position at $(x_0 = -25, y_0 = 3, z_0 = 0)$, we freely evolve the ion-atom colliding system from $t = 0$ fs up to $t = 2.4$ fs until the collision ends. Without the xuv pulse probing, the collision dynamics is illustrated by the upper panels of Fig. 1 for times (a) $t = 0.9$ fs, (b) $t = 1.3$ fs, and (c) $t = 1.7$ fs, respectively. These electron-probability density contours on the *x*-*y* plane show the dynamic process of charge transfer from the target H atom to the projectile D^+ ion. In Fig. 1(a), the D^+ ion has still not yet collided with the H atom, while Fig. 1(b)
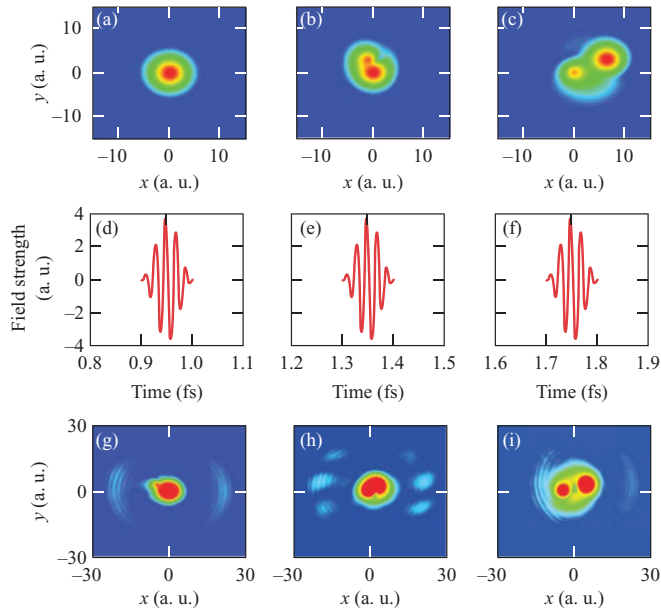
_____
[*]shu@lle.rochester.edu

FIG. 1. (Color online) The upper panels show the electron-probability density on the x-y plane during the D^+ collision with H atom at times (a) $t = 0.9$ fs, (b) $t = 1.3$ fs, and (c) $t = 1.7$ fs, respectively. The middle panels indicate the probing attosecond xuv pulses striking at times (d) $t = 0.95$ fs, (e) $t = 1.35$ fs, and (f) $t = 1.75$ fs, respectively. The lower panels [(g)–(i)] show the corresponding electron-probability density at 100 as after the probing xuv pulse strikes.
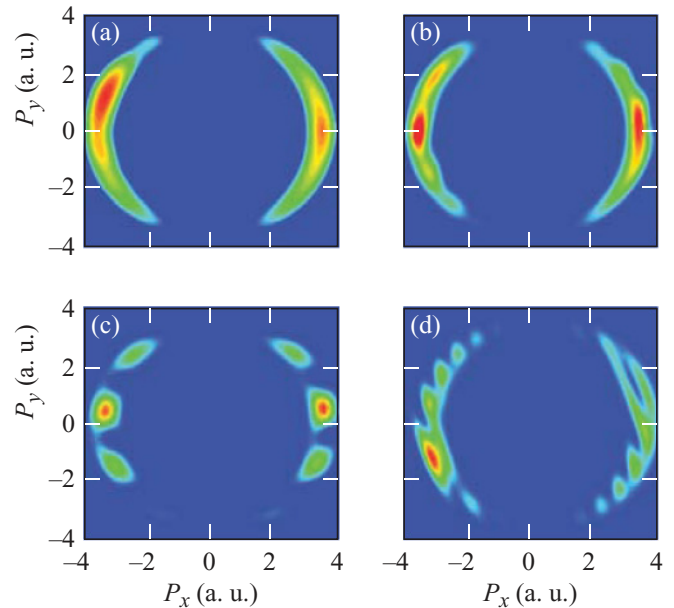

FIG. 2. (Color online) The photoelectron momentum distribution on the P_x-P_y plane, for the attosecond xuv pulse probing at different times during the collision.

captures the close-collision moment when the electron starts "hopping" around the two nuclei. It is also interesting to note in Fig. 1(h) the existence of a collision-induced vortex (at the edge of the red spot), which was recently discovered by similar time-dependent calculations [36]. In Fig. 1(c), most of the electron-wave packets have been captured by the D^+ and have moved away from the target site (the origin). Now, if the attosecond probing pulse strikes at the individual times shown by the middle panels of Fig. 1, the electron will be photoionized with certain probabilities. Allowing the photoionized electron-wave packets to freely propagate for ∼100 as after the end of the XUV pulse, we plot the spatial distribution of electron probability density on the x-y plane in the lower panels [(g)–(i)] of Fig. 1, corresponding to the probing times at Figs. 1(d)–1(f), respectively. It is clearly seen that the photoelectron exhibits the double-slit-like interference patterns in Fig. 1(h) for the case when the attosecond xuv strikes exactly at the time ($t = 1.35$ fs) of a close D^+-H collision. Before or after the moment of such a close collision, the released photoelectron has either no or much less interference, as shown by Figs. 1(g) and 1(i).

As has been well understood, the photoelectron waves coherently coming out from each site of a diatomic molecule can interfere with each other, when the photoelectron's de Brogile wavelength becomes less than the internuclear separations. Such interference leads to the double-slit-like patterns in the photoelectron angular distribution [26–28]. For the $D^+ + H$ collision system considered here, a "short-lived" molecule (HD^+) is transiently formed at the close-collision instants (e.g., at $t \sim 1.35$ fs) when the electron is coherently

populating the two sites of both H^+ and D^+. Such a transient HD^+ "molecule" can be frozen and captured by the attosecond xuv probing pulse, so that the instantly released photoelectron shows the double-slit-like interference patterns. Well before the charge transfer occurs, the photoelectron essentially comes only from the H atom, thereby leading to the absence of interference. On the other hand, if the attosecond pulse strikes well after the charge transfer is completed, the photoelectron interference significantly decreases, as is shown by Fig. 1(i). This is because the two sites are now well separated and the electron populations on the two sites are unbalanced [see Fig. 1(c)].

Performing the Fourier transform of the spatial photoelectron wave function, we obtain the momentum distribution of the outgoing photoelectron. Results are shown in Fig. 2 for the attosecond pulse probing at (a) $t = 0.95$ fs, (b) $t = 1.15$ fs, (c) $t = 1.35$ fs, and (d) $t = 1.75$ fs during the $D^+ + H$ collision. In Fig. 2(a), the D^+ has not yet collided with the H atom, so the xuv-pulse-released electron comes solely from the H atom. Therefore, there is no interference at all in the energy-conservation "momentum circle." The peak shift away from $P_y = 0$ on the left-half circle ($P_x < 0$) is due to the Coulomb focusing effect [37] on the outgoing electrons by the approaching D^+. At a slightly later time of $t = 1.15$ fs, Fig. 2(b) shows that the interference patterns start to appear as the collision begins. We now observe two additional subpeaks emerging in the momentum circle, specifically in the left-half momentum circle in Fig. 2(b). The complete double-slit interference is clearly seen in Fig. 2(c), exactly when the charge-transfer process occurs. After the charge-transfer process ends, Fig. 2(d) shows the reduced interference patterns of the photoelectron that is released at $t = 1.75$ fs. It is noted that the photoelectron momentum circle in Fig. 2(d) is overall shifted toward the positive p_x axis by ∼0.45 a.u.
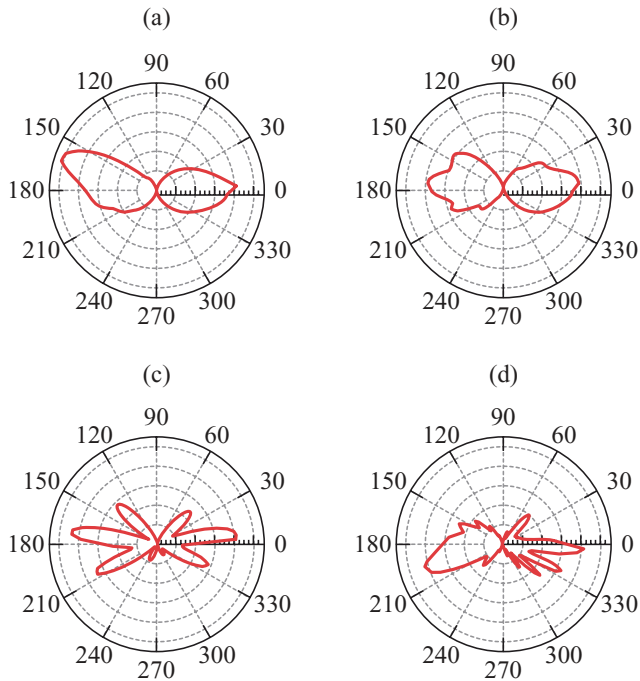
FIG. 3. (Color online) The photoelectron angular distribution corresponding to the cases depicted by Fig. 2.

(velocity of D^+) because the captured electron-wave packets are now moving with the projectile D^+ ion. Again, the Coulomb focusing effect is also seen in Fig. 2(d) in the left-half momentum circle but is now due to the H^+ at the origin.

Considering the few-cycle nature of the attosecond xuv pulse [see Figs. 1(d)–1(f)], a broadband frequency is expected for the xuv pulse field, so that the photoelectron has also a broad momentum distribution on the energy-conservation "rings," indicated by Fig. 2. Integrating the photoelectron probability density along each angle, we can plot the angular distributions in Fig. 3, which respectively correspond to the cases depicted by Fig. 2. As discussed above, the photoelectron interference visibility exactly tracks the charge-transfer dynamics. Figure 3(c) illustrates the clear
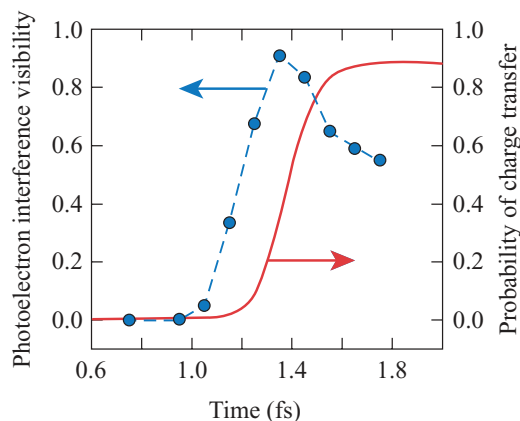

FIG. 4. (Color online) The photoelectron interference visibility (blue circles guided by the dashed line) as a function of the attosecond probing times, which peaks at the time when the charge-transfer probability (red solid line) rises.

"three-lopes" interference patterns, while the others have either reduced or no interference. We may define the photoelectron interference visibility (PIV) as PIV $= (A_P - A_V)/A_P$, where the peak amplitude (A_P) and the amplitude at the "valley" (A_V) are measured from the photoelectron angular distribution. Specifically, we have chosen the peak at $\theta \sim 180°$ and its adjacent valley ($\theta \sim 160°$) for the evaluation of PIV. For the different striking times of the probing attosecond XUV pulses, we plot in Fig. 4 the PIV with the blue circles (guided by the dashed line). The red solid line represents the charge-transfer probability as a function of the collision time. Figure 4 elucidates that the PIV peaks exactly at the time when the charge-transfer probability passes through $\sim 50\%$. Before the charge transfer occurs (e.g., $t = 0.75$ and 0.95 fs), the PIVs are all zero. After the collision occurs, the photoelectron interference visibility decreases since most of the electron-wave packets are captured by the D^+ and move away from the target site. Since the attosecond timing of the charge-transfer process is not based on the absolute contrast of these interference patterns, the proposed probe should also work for the situations having "unbalanced electron density" as in multiply charged ion-atom collisions.

Next, we briefly discuss the possible "blurring" issue when different impact parameters are considered in experiments. For this purpose, we have performed calculations by scanning the impact parameters from $y_0 = 1$, 2, 3, 4.5, and 6 a.u. to 12 a.u., with the same attosecond probe at $t = 1.35$ fs as used in Fig. 1(e). The results are summarized in Fig. 5. We found that the charge-transfer probability peaks at $y_0 = 2 - 3$ a.u., for which a similar charge distribution is around the target
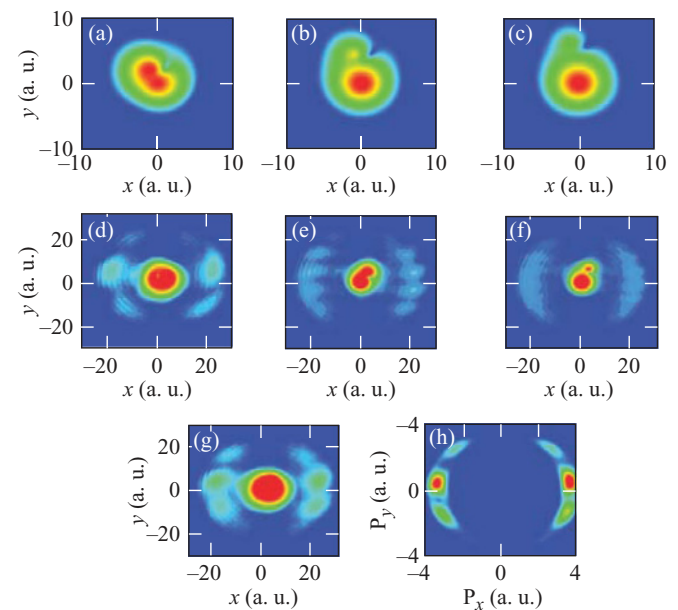

FIG. 5. (Color online) The snapshots of electron-probability densities (at $t = 1.3$ fs) for field-free D^+ (10-keV) collisions with H atom at different impact parameters (a) 2 a.u., (b) 4.5 a.u., and (c) 6 a.u., respectively. The middle panels (d)–(f) show the corresponding electron-probability density (at $t = 1.5$ fs) after the attosecond probing pulse strikes. The total electron probability density from superposing different impact-parameter calculations is plotted in (g). (h) shows the corresponding momentum distribution.

atom and the projectile ion during the attosecond probing. This can be seen from Figs. 5(a) and 1(b), while for large impact parameters ($y_0 = 4.5$ and 6 a.u.) Figs. 5(b) and 5(c) show unbalanced electron probability densities. Attosecond pulse strikes result in high-contrast and intense photoelectron interference patterns for the balanced electron-density cases [see Figs. 5(d) and 1(h) at $y_0 = 2$ and 3 a.u.], while unbalanced electron densities give much lower contrast and weak interference features indicated by Figs. 5(e) and 5(f). For the two extreme cases at $y_0 = 1$ and 12 a.u., there are no interference features. Overall, the interference patterns are dominated by the probable charge transfer at $y_0 = 2 - 3$ a.u. Now, if we superpose all the calculated results for these different y_0, we can still see the interference pattern that is shown in Fig. 5(g). The final photoelectron momentum contour plot in Fig. 5(h) indeed illustrates the interference peaks. Finally, we briefly discuss how one may synchronize the atomic collision process with the probe pulse. Energetic and monochromatic ions, emitted from the back surface of a thin foil driven by intense laser pulses, have been experimentally demonstrated in recent years [38]. If one split such an intense pulse into two pulses, of which one pulse is used to drive the ion production and the other is to produce the xuv attosecond pulse, then the synchronization between ion-atom collisions and the probe pulse can be realized. Other synchronization methods may also be stimulated by the proposed attosecond probe.

In summary, we have demonstrated that the ultrafast charge-transfer dynamics in atomic collisions can be mapped out in real time using time-delayed attosecond xuv pulses. As the projectile ion approaches the target atom, the atomic electron "hops" around the nuclei, which can be viewed as a "transient molecule." Being struck by an intense attosecond xuv pulse, the delocalized electron can be instantly photoionized from both the projectile and target sites. Such outgoing photoelectron waves will interfere with each other and double-slit-like interference patterns can be formed in the photoelectron angular spectrum. If the attosecond xuv pulse strikes well before or after the collision, there will be either reduced or no photoelectron interference. Therefore, the visibility of photoelectron interference is a timing indicator of the dynamic charge-transfer process in atomic collisions. Peeking into such ultrafast collisional processes would enhance our understanding on basic atomic physics, which may further benefit the temporal control of collisional reactions in physical and chemical systems.

[1] M. Drescher *et al.*, Science **291**, 1923 (2001).
[2] P. M. Paul *et al.*, Science **292**, 1689 (2001).
[3] X. Feng *et al.*, Phys. Rev. Lett. **103**, 183901 (2009).
[4] Z. Chang *et al.*, Phys. Rev. Lett. **79**, 2967 (1997).
[5] N. Milosevic, A. Scrinzi, and T. Brabec, Phys. Rev. Lett. **88**, 093905 (2002).
[6] T. Brabec and F. Krausz, Rev. Mod. Phys. **72**, 545 (2000).
[7] A. D. Bandrauk, J. Manz, and M. J. J. Vrakking, Chem. Phys. **366**, 1 (2009), and references therein.
[8] P. Agostini and L. F. DiMauro, Rep. Prog. Phys. **67**, 813 (2004).
[9] P. B. Corkum and F. Krausz, Nat. Phys. **3**, 381 (2007).
[10] P. B. Corkum and Z. Chang, Opt. Photon. News **19**, 24 (2008).
[11] F. Krausz and M. Ivanov, Rev. Mod. Phys. **81**, 163 (2009).
[12] M. Drescher *et al.*, Nature (London) **419**, 803 (2002).
[13] E. Goulielmakis *et al.*, Science **305**, 1267 (2004).
[14] S. Gräfe, V. Engel, and M. Y. Ivanov, Phys. Rev. Lett. **101**, 103001 (2008).
[15] S. X. Hu and L. A. Collins, Phys. Rev. Lett. **96**, 073004 (2006).
[16] T. Morishita, S. Watanabe, and C. D. Lin, Phys. Rev. Lett. **98**, 083003 (2007).
[17] S. X. Hu and L. A. Collins, J. Mod. Opt. **54**, 943 (2007).
[18] S. Sukiasyan *et al.*, Phys. Rev. Lett. **102**, 223002 (2009).
[19] M. A. Lysaght, P. G. Burke, and H. W. van der Hart, Phys. Rev. Lett. **102**, 193001 (2009).
[20] T. Zuo, A. D. Bandrauk, and P. B. Corkum, Chem. Phys. Lett. **259**, 313 (1996).

[21] S. X. Hu and L. A. Collins, Phys. Rev. Lett. **94**, 073004 (2005); F. He, A. Becker, and U. Thumm, *ibid.* **101**, 213002 (2008).
[22] S. X. Hu and L. A. Collins, Phys. Rev. A **73**, 023405 (2006); S. X. Hu and L. A. Collins, J. Phys. B **39**, L185 (2006).
[23] S. Baker *et al.*, Science **312**, 424 (2006).
[24] A.-T. Le *et al.*, Phys. Rev. A **80**, 013401 (2009).
[25] S. Haessler *et al.*, Nat. Phys. **6**, 200 (2010).
[26] S. X. Hu, L. A. Collins, and B. I. Schneider, Phys. Rev. A **80**, 023426 (2009).
[27] K.-J. Yuan, H. Z. Lu, and A. D. Bandrauk, Phys. Rev. A **80**, 061403(R) (2009).
[28] D. A. Horner *et al.*, Phys. Rev. Lett. **101**, 183002 (2008).
[29] B. H. Bransden and M. R. C. McDowell, *Charge Exchange and the Theory of Ion-Atom Collisions* (Clarendon, Oxford, 1992).
[30] M. S. Pindzola *et al.*, Phys. Rev. A **72**, 062703 (2005).
[31] B. I. Schneider, L. A. Collins, and S. X. Hu, Phys. Rev. E **73**, 036708 (2006).
[32] S. X. Hu, Phys. Rev. E **81**, 056705 (2010).
[33] S. X. Hu and L. A. Collins, Phys. Rev. A **71**, 062707 (2005).
[34] S. X. Hu, Phys. Rev. Lett. **98**, 133201 (2007).
[35] S. X. Hu, Phys. Rev. A **74**, 062716 (2006).
[36] J. H. Macek *et al.*, Phys. Rev. Lett. **102**, 143201 (2009).
[37] T. Brabec, M. Yu. Ivanov, and P. B. Corkum, Phys. Rev. A **54**, R2551 (1996).
[38] H. Schwoerer *et al.*, Nature (London) **439**, 445 (2006), and references therein.